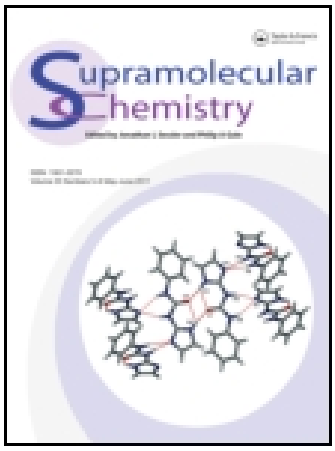

Supramolecular Chemistry
Publication details, including instructions for authors and subscription information:
http://www.tandfonline.com/loi/gsch20

# Thermotropic behaviour, self-assembly and photophysical properties of a series of squaraines

Maher A. Qaddoura [a], Kevin D. Belfield [a b], Paul Tongwa [c], Jessica E. DeSanto [c], Tatiana V. Timofeeva [c] & Paul A. Heiney [d]

[a] Department of Chemistry, University of Central Florida, Orlando, FL, 32816, USA

[b] CREOL, The College of Optics & Photonics, University of Central Florida, Orlando, FL, 32816, USA

[c] Department of Biology & Chemistry, New Mexico Highlands University, Las Vegas, NM, 87701, USA

[d] Department of Physics and Astronomy, University of Pennsylvania, Philadelphia, PA, 19104, USA

Published online: 03 Nov 2011.

To cite this article: Maher A. Qaddoura, Kevin D. Belfield, Paul Tongwa, Jessica E. DeSanto, Tatiana V. Timofeeva & Paul A. Heiney (2011) Thermotropic behaviour, self-assembly and photophysical properties of a series of squaraines, Supramolecular Chemistry, 23:11, 731-742, DOI: 10.1080/10610278.2011.622391

To link to this article: http://dx.doi.org/10.1080/10610278.2011.622391

*Supramolecular Chemistry*
Vol. 23, No. 11, November 2011, 731–742

Taylor & Francis
Taylor & Francis Group

# Thermotropic behaviour, self-assembly and photophysical properties of a series of squaraines

Maher A. Qaddoura[a], Kevin D. Belfield[a,b]*, Paul Tongwa[c], Jessica E. DeSanto[c], Tatiana V. Timofeeva[c] and Paul A. Heiney[d]

[a]*Department of Chemistry, University of Central Florida, Orlando, FL 32816, USA;* [b]*CREOL, The College of Optics & Photonics, University of Central Florida, Orlando, FL 32816, USA;* [c]*Department of Biology & Chemistry, New Mexico Highlands University, Las Vegas, NM 87701, USA;* [d]*Department of Physics and Astronomy, University of Pennsylvania, Philadelphia, PA 19104, USA*

(*Received 6 July 2011; final version received 26 August 2011*)

A series of squaraine dyes, based on 2,4-bis[4-(*N,N*-di-*n*-alkylamino)-2-hydroxyphenyl] squaraine including ethyl, propyl, butyl, pentyl, hexyl and heptyl derivatives, were synthesised by condensation of the corresponding 4-(*N,N*-di-*n*-alkylamino)-2-hydroxyphenol with squaric acid. The thermal behaviour of the series was recorded using both thermogravimetic analysis and differential scanning calorimetry while their crystalline structures were elucidated via single-crystal X-ray diffraction. The length of the alkyl chain proved to have a significant effect on both the thermotropic behaviour and the crystalline structure of the squaraine series. Two derivatives, butyl and heptyl, revealed the presence of liquid crystalline mesophases, smectic and nematic, respectively, which were confirmed and characterised via polarised light microscopy and X-ray diffraction. Several of the derivatives formed H- and/or J-aggregates upon thin film formation via spin coating before and after the thermal annealing treatment as indicated by UV–vis spectroscopy. The molecular and crystal structure, aggregation and thermal behaviour provide insight into the supramolecular assembly of this important class of materials. Photophysical measurements revealed large molar absorptivity, reasonably high fluorescence quantum yields and significant fluorescence anisotropy by making these derivatives suitable candidates for a number of electro-optic and photonics applications.

**Keywords:** squaraine dyes; crystalline structure; liquid crystalline phase; H-aggregates; J-aggregates; fluorescence anisotropy



## Introduction

Squaraine dyes have been a subject of extensive investigation due to their applications in a number of important fields such as bio-imaging probes, bio-conjugation, second generation photosensitisers for photodynamic therapy, second harmonic-generating organic dyes, two-photon absorbing materials with large cross-section values and light harvesting and photoconductor materials in photovoltaic cells (*1*). While a large number of patents and papers has appeared regarding their applications (*2–10*), limited work has been reported concerning their thermotropic behaviour including their liquid crystalline (LC) properties and the correlation of the crystalline structure to both solid-state aggregation and to their photophysical properties (*11*).

The squaraine dyes that are the subject of this research have a donor–acceptor–donor chromophore characterised by sharp and intense absorption bands in the long wavelength visible accompanied by red to near-IR fluorescence in liquid solution. They can be synthesised by condensation of electron-rich aromatics, such as *N,N*-dialkylaniline, phenols, benzothiazoles and pyrroles with squaric acid (*4*). One of the fundamental electron-rich structures that have been reported is based on *N,N*-dialkylaniline derivatives that have paved the way to construct a variety of squaraine dyes (*12–14*). One of these derivatives emanates from 3-(dialkylamino)phenol and has been employed to produce relatively stable squaraine dyes for different studies including aggregation (*15*, *16*) and sublimation (*17*).

Although several compounds based on 3-(dialkylamino)phenol, such as methyl, ethyl, propyl and butyl derivatives of 2,4-bis [4-(*N,N*-dialkylamino)-2-hydroxyphenyl] squaraine (*18*, *19*), were investigated for their fluorescence and aggregation properties in solution, very limited work has been devoted to both their supramolecular organisation in the solid state and even less to their thermotropic LC behaviour. In this work, the series is expanded to include three new compounds, i.e. pentyl, hexyl and heptyl derivatives, along with a comprehensive investigation on their thermal behaviour and self-assembly including LC properties. The photophysical properties of the entire series (ethyl to heptyl) were also investigated (Chart 1).

*Corresponding author. Email: belfield@ucf.edu

ISSN 1061-0278 print/ISSN 1029-0478 online

http://dx.doi.org/10.1080/10610278.2011.622391
http://www.tandfonline.com

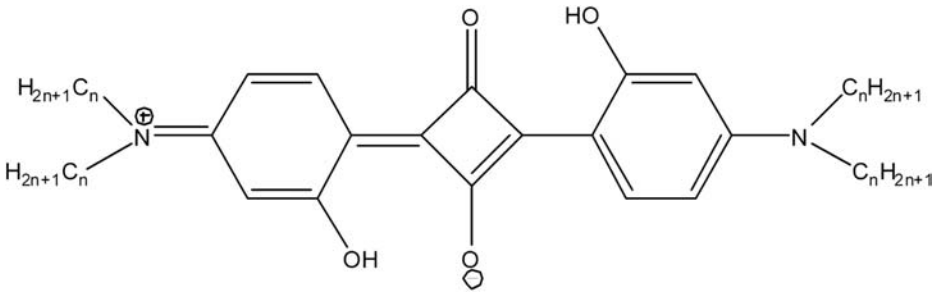


Chart 1. $n = 2$: **SQC2OH**; $n = 3$: **SQC3OH**; $n = 4$: **SQC4OH**; $n = 5$: **SQC5OH**; $n = 6$: **SQC6OH**; $n = 7$: **SQC7OH**.

## Experimental

### *Materials*

1-Bromopropane (99%), 1-bromohexane (99% +), 1-bromoheptane (99%), 3-(di-*n*-ethyamino)phenol (99%), 3-(di-*n*-butylamino)phenol (99%), aminophenol (99%) and 3,4-dihydroxy-3-cyclobutane-1,2-dione (99%) were purchased from Acros Organics and Aldrich, USA; 1-bromopentane was obtained from Eastman Organic Chemicals, USA and sodium carbonate (99.5%) was purchased from Spectrum. 3-(Di-*n*-propylamino)phenol, 3-(di-*n*-pentylamino)phenol, 3-(di-*n*-hexylamino)phenol and 3-(di-*n*-heptylamino) phenol were prepared according to procedures given in the literature (*20*). **SQC2OH**, **SQC3OH** and **SQC4OH** were prepared by the previously reported methods (*21*, *18*).

### *Synthesis*

#### *2,4-Bis [4-(*N,N-*(di-*n-*pentylamino)-2-hydroxyphenyl] squaraine (**SQC5OH**)*

3-(Di-*n*-pentylamino)phenol (2.66 g, 11.2 mmol) was added to 3,4-dihydroxy-3-cyclobutane-1,2-dione (0.7 g, 6.1 mmol) dissolved in 20 ml of 1:1 butanol and toluene. After 7 h of reflux, the reaction mixture was cooled to room temperature and the precipitate was obtained. The solvent was removed on a rotary evaporator *in vacuo* and the product was recrystallised in $CHCl_3$ to yield 1.02 g (60%) of 2,4-bis [4-(*N, N*-dipentylamino)-2-hydroxyphenyl] squaraine as bright yellowish to greenish crystals. MP = 185°C. $^1$H NMR 300 MHz ($\delta$ ppm tetramethylsilane (TMS), $CDCl_3$): 0.94 (m, 12H, $CH_3$), 1.18 (m, 8H, $CH_2$), 1.34 (m, 8H, $CH_2$), 1.62 (m, 8H, $CH_2$), 3.36 (m, 8H, $CH_2$), 6.1 (d, $J = 3$ Hz, 2H), 6.3 (dd, $J = 3$ Hz), 7.87 (d, $J = 3$ Hz, 2H) and 8.01 (d, $J = 9$ Hz, 2H). $^{13}$C NMR ($\delta$ ppm TMS, $CDCl_3$): 13.85, 22.03, 26.91, 28.84, 51.57, 98.24, 107.37, 109.31, 132.5, 155.49, 163.8, 172 and 183. liquid chromatography-mass spectrometry (LC-MS): theoretical $M^+ = 576.3922$, found $M/z = 576.3895$.

#### *2,4-Bis [4-(*N,N-*di-*n-*hexylamino)-2-hydroxyphenyl] squaraine (**SQC6OH**)*

3-(Di-*n*-hexylamino)phenol (1.3 g, 4.7 mmol) was added to 3,4-dihydroxy-3-cyclobutane-1,2-dione (0.44 g, 3.86 mmol) in 20 ml of 1:1 butanol and toluene. After 6 h of reflux, the reaction mixture was cooled to room temperature and the precipitate was obtained. The solvent was removed on a rotary evaporator *in vacuo* and the product was recrystallised in $CHCl_3$ to yield 1.2 g (81%) of 2,4-bis [4-(*N,N*-dihexylamino)-2-hydroxyphenyl] squaraine as shiny green crystals. MP = 135°C. $^1$H NMR 300 MHz ($\delta$ ppm TMS, $CDCl_3$): 0.93 (m, 12H, $CH_3$), 1.32 (m, 24H, $CH_2$), 1.63 (m, 8H, $CH_2$), 3.36 (q, 8H, $CH_2$), 6.10 (d, $J = 3$ Hz, 2H), 6.32 (dd, $J = 3$ Hz), 7.88 (d, $J = 3$ Hz, 2H) and 8.00 (d, $J = 9$ Hz, 2H). $^{13}$C NMR ($\delta$ ppm TMS, $CDCl_3$): 13.6, 22.3, 26.4, 31.5, 51.04, 98.5, 107.4, 109.8, 132.3, 156.0, 163.8, 164.5, 171.2, 173.1 and 182.6. LC-MS: theoretical $M^+ = 632.4548$, found $M/z = 632.4537$.

#### *2,4-Bis [4-(*N,N-*di-*n-*heptylamino)-2-hydroxyphenyl] squaraine (**SQC7OH**)*

3-(Di-*n*-heptylamino)phenol (2.08 g, 7.56 mmol) was added to 3,4-dihydroxy-3-cyclobutane-1,2-dione (0.39 g, 3.4 mmol) dissolved in 20 ml of 1:1 butanol and toluene. After 6 h of reflux, the reaction mixture was cooled to room temperature and the precipitate was obtained. The solvent was removed on a rotary evaporator *in vacuo* and the product was recrystallised from $CHCl_3$ to yield 1.4 g (60%) of 2,4-bis [4-(*N,N*-diheptylamino)-2-hydroxyphenyl] squaraine as bright yellowish to greenish crystals. MP = 119°C. $^1$H NMR 300 MHz ($\delta$ ppm TMS, $CDCl_3$): 0.90 (m, 12H, $CH_3$), 1.32 (m, 32H, $CH_2$), 1.60 (m, 8H, $CH_2$), 3.37 (q, 8H, $CH_2$), 6.11 (d, $J = 3$ Hz, 2H), 6.31 (dd, $J = 3$ Hz), 7.88 (d, $J = 3$ Hz, 2H) and 8.03 (d, $J = 9$ Hz, 2H). $^{13}$C NMR ($\delta$ ppm TMS, $CDCl_3$): 14.29, 22.3, 26.4, 27.8, 29.3, 31.5, 51.6, 98.7, 107.4, 109.6, 131.8, 156.0, 163.5, 164.0, 171.7, 173.1 and 182.6. LC-MS: theoretical $M^+ = 688.5174$, found $M/z = 688.5189$.

### *Instrumentation and methods*

Thermogravimetric analysis (TGA) was carried out using a TGA Q5000 thermogravimetric analyser (TA Instruments) at a heating rate of 10°C/min. The thermotropic behaviours of all compounds were determined by a

combination of differential scanning calorimetry (DSC) and polarised optical microscopy. A TA Instruments Q1000 DSC was used to determine the thermal transitions during heating and cooling cycles; all heating and cooling rates were 10°C/min; thermal transitions were read from reproducible second scans. An Olympus BX51 polarised optical microscope (magnification $\times 40$) equipped with both a DP70 microscope digital camera and an Instec HCS302 heating/cooling stage was used to detect and image the phase transitions by observing thin samples between a clean glass slide and a cover slip.

*Single-crystal X-ray diffraction study*

Single crystals of the series of squaraine dyes were grown by slow evaporation from $CHCl_3$ for single-crystal X-ray diffraction, which was carried out with a Bruker SMART APEX II diffractometer with CCD area detector (graphite monochromated Mo-K$\alpha$ radiation, $\lambda = 0.71073$ Å) and $\omega$-scans with a 0.5° step in $\omega$ at 100 K. The semi-empirical method SADABS was applied for absorption correction for all compounds; data reduction and further calculations were performed using Bruker SAINT + and SHELXTL NT program packages. The structures were solved by direct methods and refined by the full-matrix least-squares technique against $F^2$ with the anisotropic temperature parameters for all non-hydrogen atoms except **SQC5OH**, where the disordered C-atoms were refined in isotropic approximation because of the disorder of the side chains. All hydrogen atoms were calculated from the geometrical point of view within the riding model except for the hydroxyl groups in **SQC3OH** and **SQC4OH**, where they were located from the Fourier electron density synthesis. In the three compounds, the hydroxyl groups are disordered over two positions with the occupancies 0.75:0.25 in **SQC4OH**, 0.85:0.15 in **SQC5OH** and 0.57:0.43 in **SQC6OH** and alternate with hydrogens in these positions. In the molecule **SQC5OH** that resides on an inversion centre, two alkyl side chains are disordered over two positions with the occupancies 0.60:0.40 and 0.56:0.44, respectively, while in the molecule **SQC6OH** which occupies general position three of four alkyl chains are disordered over two positions with the occupancies 0.54:0.46; 0.63:0.37 and 0.63:0.37, respectively. The details of crystal structures are given in the Supporting Information, available online. The X-ray data and the details of the structure refinement are summarised in Table S1; the selected geometry parameters are given in Table S2 and the hydrogen-bonding geometry is given in Table S3. Crystallographic data for the structures in this paper have been deposited with the Cambridge Crystallographic Data Centre as supplementary publication numbers CCDC 829763–829767. Copies of the data can be obtained, free of charge, on application to CCDC, 12 Union Road, Cambridge CB2 1EZ, UK (Fax: +44-(0)1223-336033 or e-mail: deposit@ccdc.cam.ac.uk).

*Powder and LC phase X-ray diffraction studies*

Temperature-dependent X-ray diffraction measurements of powder samples employed a Bruker-Nonius FR591 fine-focus generator with a Cu target ($\lambda = 1.542$ Å), Osmic confocal optics and a Bruker HiStar wire detector. Measurements were obtained at a fixed sample–detector distance of 11 cm. The scattered intensity was recorded for scattering vectors in the range $0.2\,\text{Å}^{-1} \leq q\ (= 4\pi \sin(\theta)/\lambda) \leq 1.7\,\text{Å}^{-1}$. Measurements were obtained between room temperature and the clearing point upon both heating and cooling. The heating and cooling rates were both 10°C/min, and the data were collected for 5 min at each temperature. The primary data analysis was carried out using Datasqueeze (http://www.datasqueezesoftware.com). Thin films were prepared by spin coating a 2% solution of the dye in $CHCl_3$ at 2000 rpm.

Absorbance measurements were obtained using Agilent 8453 UV–vis spectrophotometer; the steady-state emission and excitation anisotropy studies were carried out using a Photon technologies, Inc. (PTI) QuantaMaster spectrofluorimeter in 10 mm spectrofluorometric quartz cuvettes with $C \sim 10^{-6}$ M and Rhodamine 6G as reference. Fluorescence spectra were corrected for the spectral responsivity of the PTI emission monochromator and photomultiplier tube. Gas chromatography-mass spectrometry analyses were conducted in the Mass Spectrometry Services, Chemistry Department at the University of Florida. $^1$H and $^{13}$C NMR analyses were carried out in $CDCl_3$ (referenced to TMS at $\delta$ 0.0 ppm) using Varian NMR spectrometers (500 or 300 MHz for $^1$H and 75 MHz for $^{13}$C).

## Results and discussions

A series of six squariane dyes varying in the length of their peripheral alkyl groups were investigated for their thermal properties, phase transitions, crystalline structure, aggregation and photophysical properties. The synthetic procedure for their preparation involved an etherification with the corresponding 1° alkyl bromide with 3-aminophenol, followed by a subsequent condensation reaction between the 3-(di-*n*-alkylamino)phenol derivative with squaric acid in a mixture of butanol and toluene (*14*, *22*) as shown in Scheme 1.

### *The crystal structures*

Crystal structures of **SQC2OH** and mono-hydroxylated analogue of **SQC4OH** were reported previously (*23*, *24*). We present herein the first report on the crystal structures of **SQC3OH**, **SQC4OH, SQC5OH**, **SQC6OH** and

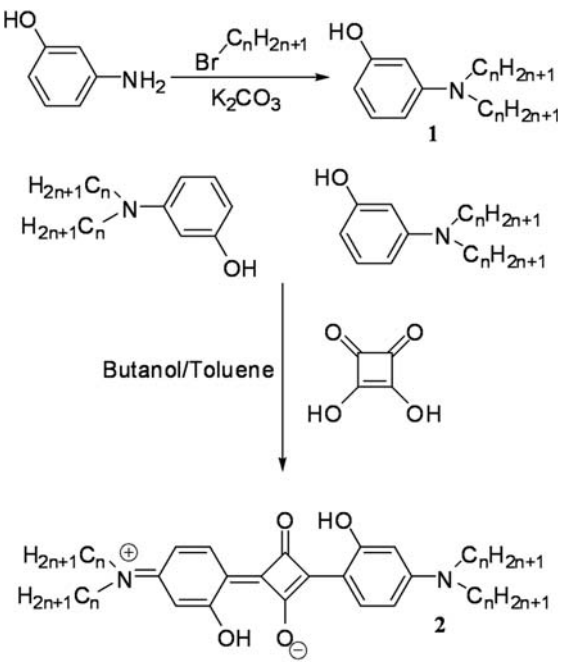


Scheme 1. The general procedure to synthesise the series of 2,4-bis[4-(*N,N*-di-*n*-alkylamino)-2-hydroxyphenyl] squaraines; $n = 2$: **SQC2OH**; $n = 3$: **SQC3OH**; $n = 4$: **SQC4OH**; $n = 5$: **SQC5OH**; $n = 6$: **SQC6OH**; $n = 7$: **SQC7OH**.

**SQC7OH**. The crystal structure of **SQC2OH** was not repeated as we were unable to obtain suitable single crystals. Of the compounds studied, only **SQC3OH** crystallises in the non-centrosymmetric $P2_1$ space group, while four other compounds crystallise in the centrosymmetric space groups $P2_1/c$ (**SQC4OH**, **SQC6OH**), $P2_1/n$ (**SQC5OH**) and $P$-1 (**SQC7OH**). The molecules **SQC3OH** and **SQC6OH** occupy general positions with the whole molecule in the asymmetric unit, while **SQC4OH**, **SQC5OH** and **SQC7OH** reside on inversion centres. The planarity of the central core that includes a four-membered ring and two phenyl rings is sustained by the presence of the conjugation and the hydrogen bonding between the hydroxyl groups and the carbonyl atoms in which the geometry parameters are very close in all molecules except **SQC6OH** where deviations were caused by the crystal structure disorder. The C—C as well as C—O distances in the squaraine central fragment reflect its high symmetrical electron distribution (Supporting Information, available online, Table S2). The squaraine structures also demonstrate a quinoid character of both phenyl substituents that have donor and acceptor groups in *para* positions. Despite the similarity of the central molecular fragment and its high symmetry, the molecules differ significantly by the orientations and conformations of the flexible alkyl substituents. The short alkyl chains of **SQC3OH** and **SQC4OH** located on both sides of the central core have different orientations and conformations. In the molecule **SQC5OH**, significant deviations of disordered pentyl chains in 'up' and 'down' directions relative to the core were observed. In **SQC6OH**, two hexyl side chains are extended in the plane of the main core, while the other two are oriented nearly perpendicular to the central planar fragment. In the molecule **SQC7OH**, the heptyl chains are located in planes nearly parallel to the central core 'above' and 'below' this plane.

It is known that in some cases solid crystalline precursors can demonstrate a 3D structure similar to 1D or 2D structures of LC phases. The packing in the crystal might also demonstrate the type of molecular associates that can be formed by certain materials in solution. The careful analysis of the molecular packings (Figures 1 and 2) revealed some similarities within this series of compounds. The molecules **SQC3OH**, **SQC4OH** and **SQC5OH** form H-bonded ribbons at the position of the cores in one plane that might be considered as 1D associates (Figure 1). The packing of these ribbons essentially differs in **SQC3OH** and in **SQC4OH** and **SQC5OH**. The short propyl chains in **SQC3OH** do not impede the stacking of the parallel ribbons in the partially overlapping mode giving rise to the layers strengthened by weak CH···O hydrogen bonding. The layers are packed in a herringbone mode. In the crystals **SQC4OH** and **SQC5OH**, the butyl and pentyl side chains prevent the overlapping of the ribbons, providing their identical herringbone arrangement in both structures being quite similar to the non-hydroxylated and mono-hydroxylated analogous of **SQC4OH** (*23*). The **SQC4OH** herringbone arrangement is also consistent with the structure previously reported using scanning tunnelling microscopy investigation (*25*).

We can speculate that similar aggregates can be formed for both **SQC6OH** and **SQC7OH** in solution but not in crystals where close packing most likely prevents such arrangement. Nonetheless, associates resembling ribbons that can be seen in both these structures (Figure 2(A), (D)). In the crystals **SQC6OH** and **SQC7OH**, the molecular cores are oriented in one direction and they are surrounded by long alkyl substituents that impede the self-association of the molecules in the planar ribbons (Figure 2). In **SQC7OH**, the CH···O bonds link the parallel molecules in the stair-case-like ribbons. Both these arrangements might be considered as a LC precursor, but our observations showed that it was realised only in **SQC7OH** that was confirmed by polarised light microscopy (PLM) texture observations.

### *Thermotropic behaviour*

The length of the peripheral alkyl group appeared to exert a profound effect on the thermal stability for each compound. It was observed that the shorter the alkyl group, the higher the decomposition temperature (Table 1). This observation can be explained by the intermolecular

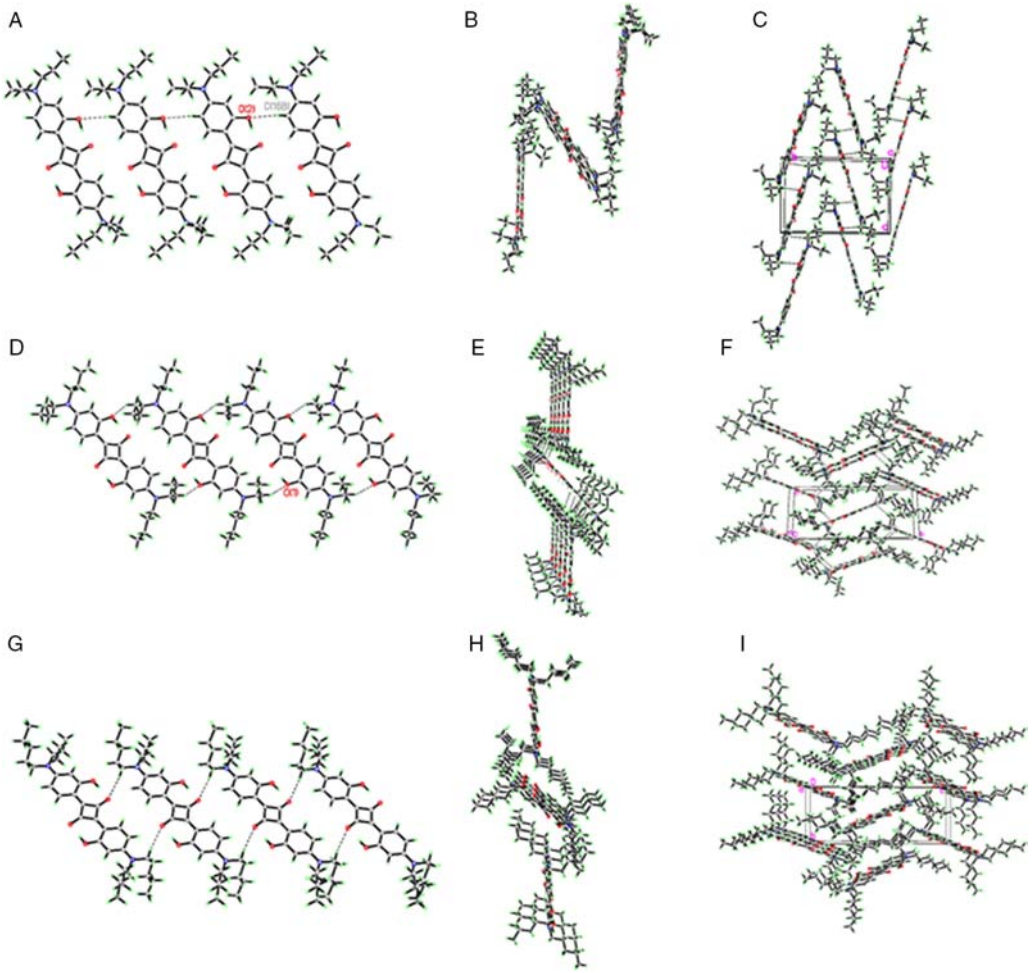


Figure 1. Fragments of crystal packing in **SQC3OH**, **SQC4OH** and **SQC5OH**. **SQC3OH**: (A) H-bonded ribbon, (B), (C) the herringbone packing of the ribbons; **SQC4OH**: (D) H-bonded ribbon, (E) herringbond arrangement of the ribbons with short CH···O contacts between them, (F) crystal packing; **SQC5OH**: (G) H-bonded ribbon, (H) herringbond arrangement of the ribbons with no evident short CH···O contacts between them, (I) crystal packing.



interactions including both hydrogen bonding and van der Waals' forces for electron-rich regions for the lower peripheral alkyl chain structure. However, by increasing the length of the hydrophobic alkyl chains, the intermolecular forces become weaker resulting in low melting points.

The thermotropic behaviour was investigated for each of the squaraine dyes using DSC (Figure 3). The *n*-propyl, *n*-pentyl and *n*-hexyl derivatives (Figure 3(B),(D),(E), respectively) revealed sharp melting transition temperatures in addition to weak crystalline transitions for *n*-pentyl (Figure 3(D)) and *n*-hexyl (Figure 3(E)) derivatives, as observed by PLM, whereas the *n*-butyl (Figure 3(C)) and *n*-heptyl (Figure 3(F)) analogues exhibited phase transitions. Only the ethyl derivative did not show any melting process but rather only decomposition (Figure 3(A)).

Although the cooling cycles did not show recrystallisation for the series of squaraine compounds except for **SQC3OH** (Figure 3(B)), the PLM analysis confirmed the recrystallisation process (Figures 4–7). This behaviour may be due to the sample preparation and the container and supercooling effect. Whilst the DSC pan offered a smooth and clean surface that hindered the alkyl squaraines to pack and recrystallise owing to both the smaller surface area and smaller London attractions of the branched alkyl chain (*26*). This has been previously reported, possibly involving the reorientational dynamics during the supercooling process (*27*, *28*) and increased mobility of the alky chains (*29*). The surface of the glass slides used in PLM likely caused the induction of both the nucleation and the crystal growth process due to surface scoring or defects during the cooling process at room temperature. However, upon cooling very slowly at

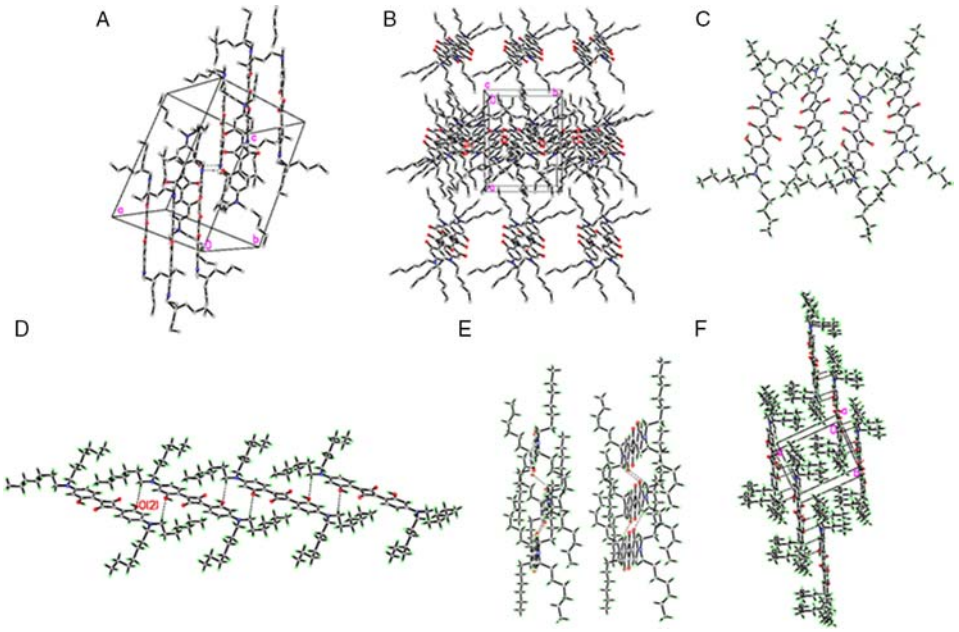


Figure 2. Fragments of crystal packing for **SQC6OH** and **SQC7OH**. **SQC6OH**: (A) chain of corrugated molecules, (B), (C) the alignment of the molecules in the crystal, H-atoms are omitted; **SQC7OH**: (D), (E) H-bonded stair-case ribbon – top and side views, (F) crystal packing.

Table 1. Summary of the thermotropic properties of the squaraine derivatives.

| | Decomposition (°C) | Phase transition-1 (°C) | Enthalpy (KJ mol$^{-1}$) | Phase transition-2 (melting point, °C) | Enthalpy (KJ mol$^{-1}$) |
|---|---|---|---|---|---|
| **SQC2OH** | 240 | n/a | n/a | n/a | n/a |
| **SQC3OH** | 227 | n/a | n/a | 221 | 53.4 |
| **SQC4OH** | 224 | 164 | 9.08 | 196 | 37.6 |
| **SQC5OH** | 226 | n/a | n/a | 185 | 50.4 |
| **SQC6OH** | 228 | n/a | n/a | 135 | 33.4 |
| **SQC7OH** | 232 | 99 | 24.5 | 119 | 24.8 |

1°C/min, the phase transition signals for **SQC7OH** began to appear on the cooling curve as seen in Figure 4.

The **SQC3OH** squaraine also revealed a sharp melting point followed by recrystallisation upon cooling; any further heating above 221°C resulted in abrupt decomposition (Figure 3(B)). It was discovered that **SQC4OH** and **SQC7OH** exhibited LC phases; the mesophase occurrence is dependent on the intrinsic properties of the dye such as the conformation and arrangement of the molecule and the intermolecular interactions. Typically, the generation of a LC phase implies the loss of long-range crystalline order. A smectic phase is characterised by short-range, liquid-like positional order within well-defined sheets or layers, while in a nematic phase the molecules have long-range orientational order of the long axis director but only short-range positional order. Upon further heating all order is lost, forming the isotropic liquid (*30*, *31*).

Compound **SQC4OH** displayed two phase transitions upon heating, as seen in Figure 3(C). Although crystallisation upon cooling was not observed by DSC, the phase transition was clearly observed by PLM upon cooling (Figure 6(C)). The transition temperatures and the enthalpy of transitions, determined by DSC, are shown in Table 1. At 164°C, 9.08 kJmol$^{-1}$ of energy was released attributed to the disruption of the translational order of the crystal lattice, likely ascribed to the crystalline-smectic-like mesophase. However, at 196°C, a significantly larger enthalpy value (37.6 kJmol$^{-1}$) was recorded due to major disruption in the molecular packing to both the positional and orientational order, forming anisotropic liquid. The mesophase for **SQC4OH** was observed and identified by the texture morphology observed by PLM upon cooling of the molten crystals. The principle of the phase identification depends on observing the microscopic textures by PLM, characterised by the defects, the elastic

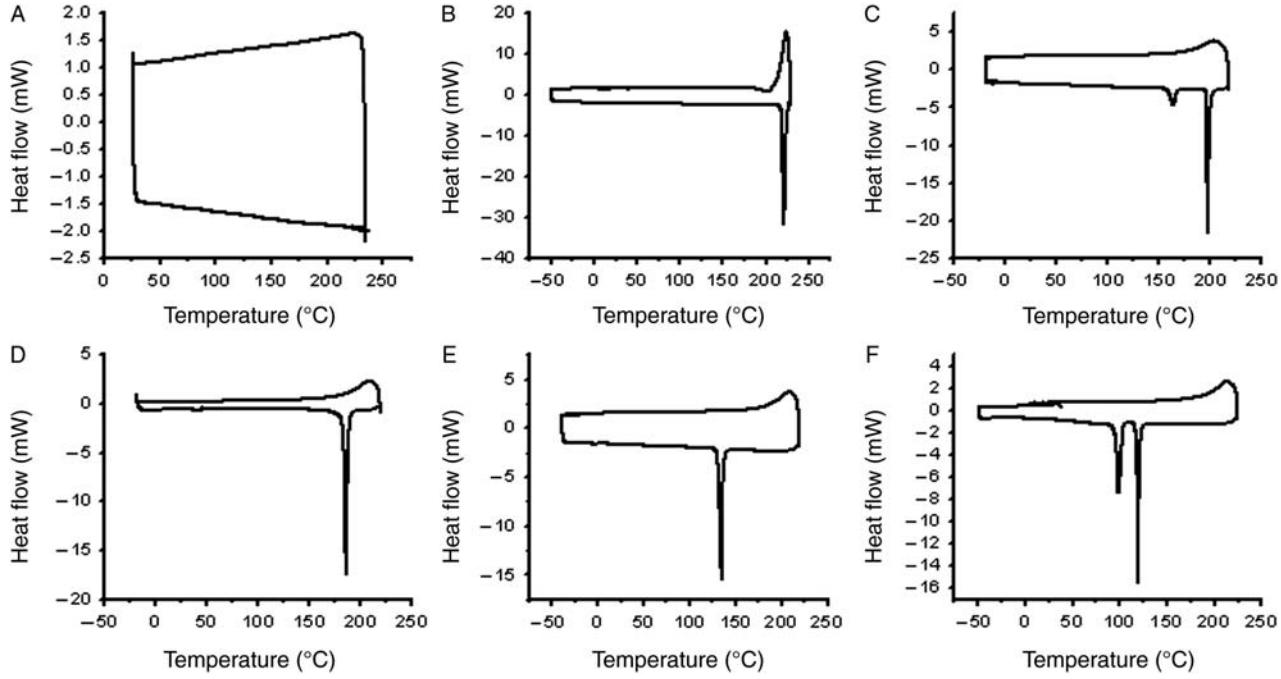


Figure 3. The thermotropic behaviour for the series of squaraine dyes. (A) The DSC thermogram for **SQC2OH**, no melting point was detected, it decomposed at 240°C. (B) The DSC thermogram for **SQC3OH**, it exhibited a melting point at 221°C followed by recrystallisation at 220°C. (C) DSC thermogram for **SQC4OH** revealed a phase transition at 164°C and a melting temperature at 196°C. (D) DSC thermogram for **SQC5OH** showed a melting point at 185°C. (E) The DSC thermogram for **SQC6OH** exhibited a melting point at 135°C. (F) DSC thermogram for **SQC7OH** revealed a phase transition at 99°C and a melting temperature at 119°C.



deformation and the birefringence between two glass slides. The interaction of the polarised light with the topology of the defects and the deformation elasticity, in combination with the birefringence, results in characteristic texture morphology for each LC phase (*32*, *33*). When external forces are applied, e.g. shear stress on the slides during sample preparation, the difference in the bulk elasticity and the fluidity (elastic constants) for each phase results in a distinguished texture morphology (*34*). Figure 6(A) presents the growth of the mesophase from the melt upon cooling. The fan-shaped nuclei are characterised by extinction crosses that appear dark when the optical axis is parallel to either the polariser or the analyser. In Figure 6(B), the transition from the mesophase to the crystalline texture was revealed; while Figure 5(C) illustrates the crystalline texture at thin thickness exhibiting different birefringence.

The DSC for **SQC5OH** showed only a sharp melting point at 185°C as can be seen in Figure 3(D). However, PLM revealed the presence of a phase transition assumed to be between crystalline phase; the crystalline-to-

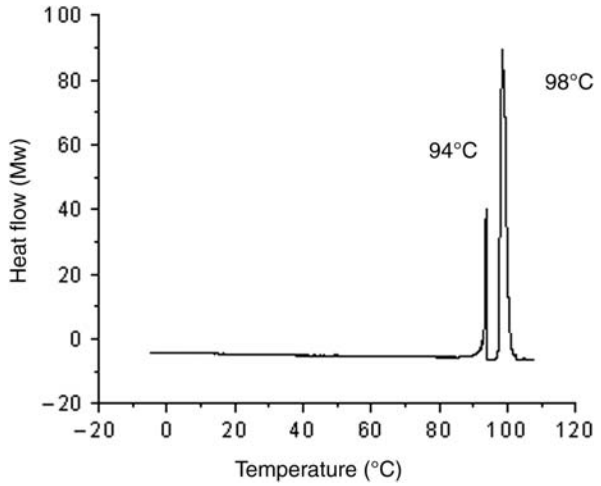


Figure 4. The DSC cooling cycle at 1°C/min for **SQC7OH** reveals the phase transitions at 98°C and 94°C.

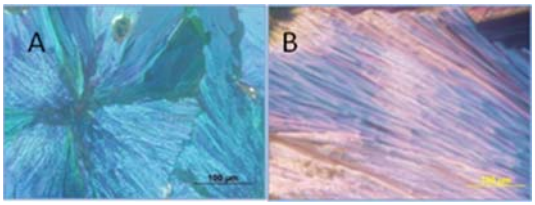


Figure 5. The recrystallisation texture of pentyl and hexyl derivatives of squaraine dyes as can be seen under PLM; the coloured texture is a result of the birefringence. (A) The crystalline texture of **SQC5OH**. (B) The crystalline texture of **SQC6OH**.

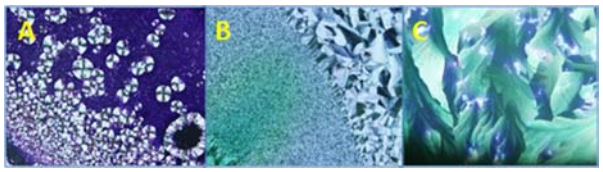


Figure 6. Phase transitions for **SQC4OH**. (A) The growth of the mesophase from the melt upon cooling at 196°C; the fan-shaped nuclei are characterised by extinction crosses that appear dark when the optical axis is parallel to either the polariser or the analyser. These extinction crosses rotate along the direction of the rotating polariser, indicating that the liquid crystal is optically positive. (B) The transition from the mesophase to the crystalline morphology at 164°C. (C) The crystalline texture morphology for thin film of **SQC4OH**.

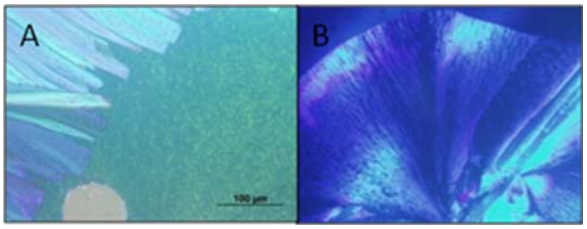


Figure 7. (A) Crystalline-to-crystalline phase transition at 140°C for **SQC5OH**; the difference in colour in both the morphologies is attributed to deformations and birefringence (the difference between extraordinary ray and ordinary ray of the polarised light when entering the sample). (B) Crystalline-to-crystalline transition for **SQC6OH** at 110°C; each phase has a slightly different type of topological defect and deformation. The interaction of the polarised light with the deformation and defect for each phase results in different path differences and birefringence.

crystalline transition can be seen in Figure 7(A). The crystal packing of **SQC5OH** (Figure 1) determined by single-crystal X-ray crystallography may provide some rationale to account for the crystalline-to-crystalline transition. This type of constrained packing impedes the molecule from undergoing considerably favourable translational and rotational effect towards forming a LC phase. However, it is only capable of undergoing a crystalline-to-crystalline transition as this requires minimum translational and rotational energy. The same argument pertains to **SQC6OH**. Similarly, **SQC6OH** not only demonstrates a sharp melting point, as can be seen in the DSC thermogram (Figure 3(E)), but also a weak phase transition when observed by PLM. The unknown phase transition is assumed to be crystalline-to-crystalline transition, see Figure 7(B).

The DSC thermogram for **SQC7OH** (Figure 3(F)) clearly demonstrates the presence of a phase transition upon heating. Although a weak transition was observed upon cooling by DSC, this phase transition was clearly evident by PLM upon cooling. The transition temperatures

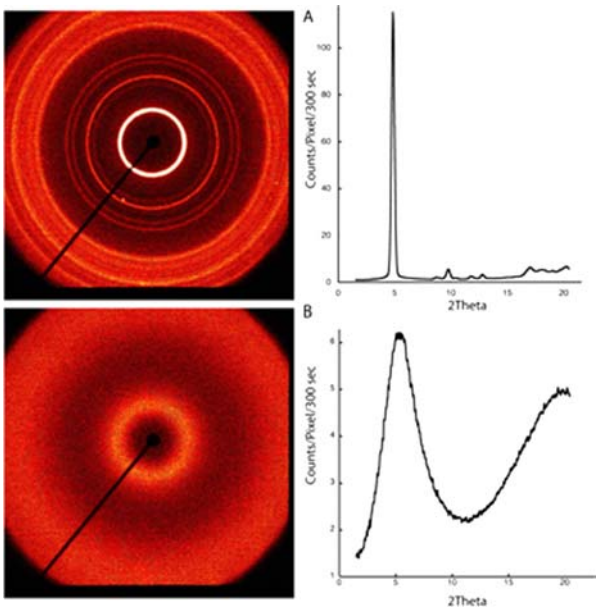


Figure 8. Powder X-ray diffraction patterns for **SQC7OH**. Left: false colour images of measured intensity; right: radial plots of circularly averaged intensity. (A) Crystalline structure at 99°C, showing Bragg peaks. (B) Nematic phase at 103°C, showing diffuse liquid-like peak at 5°(the peak at wider angle is primarily due to the glass capillary and alkyl groups).

and the enthalpy of transitions determined by DSC are shown in Table 1; at 99°C, 24.5 kJmol$^{-1}$ of energy was released due to the disruption of the translational order, which might be ascribed to the solid crystalline-mesophase transition. Furthermore, at 119°C, the energy released was 24.8 kJ mol$^{-1}$ attributable to a major disruption of the molecular packing in both the positional and orientational order to become an isotropic liquid. Powder X-ray diffraction (Figure 8) was utilised to identify and confirm the phase transitions. A crystalline phase was observed at room temperature (see Figure 7), while above 99°C a phase with a nematic-like broad peak at 0.374 Å$^{-1}$ was observed that is consistent with the DSC data. At 129°C, the signal disappeared completely, most likely due to transition to the isotropic phase.

The texture observations for **SQC7OH** were conducted using PLM upon cooling. Figure 9 shows the appearance of natural texture of the nematic phase without showing the Schlieren texture.

### *Aggregation in the solid state*

Aggregation of squaraines in the microcrystalline state has been reported for squaraine structures bearing the *N*-pyrrolidine group for xerographic applications (*35*, *36*). Spin casting of a symmetrical squaraine, 2,4-bis[4-(*N,N*-di-isobutylamino)-2,6-dihydroxyphenyl]squaraine, was investigated for enhancing the power conversion efficiency

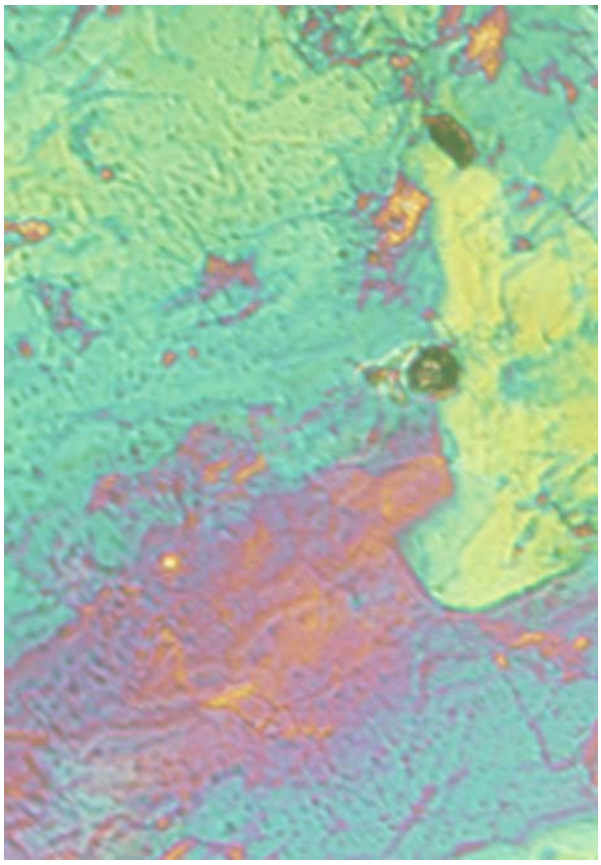

Figure 9. The natural texture of the nematic for **SQC7OH**.

for photovoltaic cells (*37*). Formation of a Langmuir–Blodgett film was utilised to study the aggregation of monolayers of selected squaraines on the surface (*15*, *38–41*). However, limited studies have been reported to systematically investigate the effect of molecular structure on the aggregation properties in solid-state films (*24*, *42–44*). Hence, we investigated the aggregation behaviour of a series of squaraine compounds in the solid state (thin films) using a spin coating method on quartz substrates to probe the effect of the peripheral alkyl chain on their aggregation behaviour before and after thermal annealing and to correlate their aggregation properties with their crystalline structures. Exciton theory was used as a model to explain the shifts of the absorption band before and after the thermal annealing process. Based on the molecular exciton theory, the angle observed between the long axis of the squaraine molecule and the straight line passing through the centre of the molecular aggregates is called the slip angle and is considered essential in determining the type of aggregates, i.e. a large slip angle results in a parallel plane-to-plane stacking and formation of a sandwich-type arrangement (H-aggregate, blue shift), whereas a smaller slip angle results in end-to-end stacking and formation of a head-to-tail arrangement (J-aggregate, red shift) (*45–47*).

One can see from Figure 10(A) that, upon spin coating of **SQC3OH**, both large slip angles and smaller ones result in multiple H-aggregates at 503 and 566 nm and J-aggregates at 732 and 787 nm compared with the monomer absorbance in $CHCl_3$ solution at 647 nm. After thermal annealing, the vibrational and the rotational energies and collisions result in a new state of equilibrium and new state of molecular arrangement manifested in a wider slip angle and formation of primarily of H-aggregates.

In Figure 10(B), a large slip angle appears dominant upon spin coating **SQC4OH**, resulting in prevailing H-aggregation at 546 nm. However, after thermal annealing, the slip angle became smaller, resulting in an H-aggregate shifted to a slightly longer wavelength (607 nm) triggering the formation of J-aggregates (767 nm).

Similarly, **SQC5OH** underwent formation of H-aggregates upon spin coating (absorption at 537 nm) while the annealing process exerted little influence on the slip angle, resulting in shifting the H-aggregate absorption from 537 to 570 nm (Figure 10(C)). Finally, both **SQC6OH** and **SQC7OH** tended to form H-aggregates in spin-coated films before and after thermal annealing without any likely change in the slip angle (Figure 10(D),(E)). The herringbone packing in **SQC3OH**, **SQC4OH** and **SQC5OH** structures may account for the capability of the molecules to change the slip angle and to shift the aggregation after thermal annealing. Otherwise, the alignment of the molecules along one direction in **SQC6OH** and **SQC7OH** may account for their inability to change the slip angle and alter aggregation after thermal annealing. These types of solid-state aggregates may be advantageous in certain electro-optic applications, e.g. in enhancing both photovoltaic cell performance and efficiency (*48*, *49*).

### *Photophysical properties*

The absorption and fluorescence emission of several symmetrical and unsymmetrical squaraines with diverse molecular entities were reported (*18*, *50*). Here, the photophysical properties for the series of squaraines based on 3-(di-*n*-alkylamino)phenol derivatives were investigated while exploring the possible effect of the peripheral alkyl chain on their photophysical properties. The series of the synthesised squaraine dyes was characterised by higher molar absorptivity, smaller Stokes shifts and relatively narrow absorption bands in solution, making this series particularly attractive for applications requiring narrow and specific excitation wavelength ranges.

Although the length of the peripheral alkyl group may slightly increase the electron-donating ability of the nitrogen atom, and, consequently, lead to an increase in the fluorescence quantum yield, this effect was negligible.

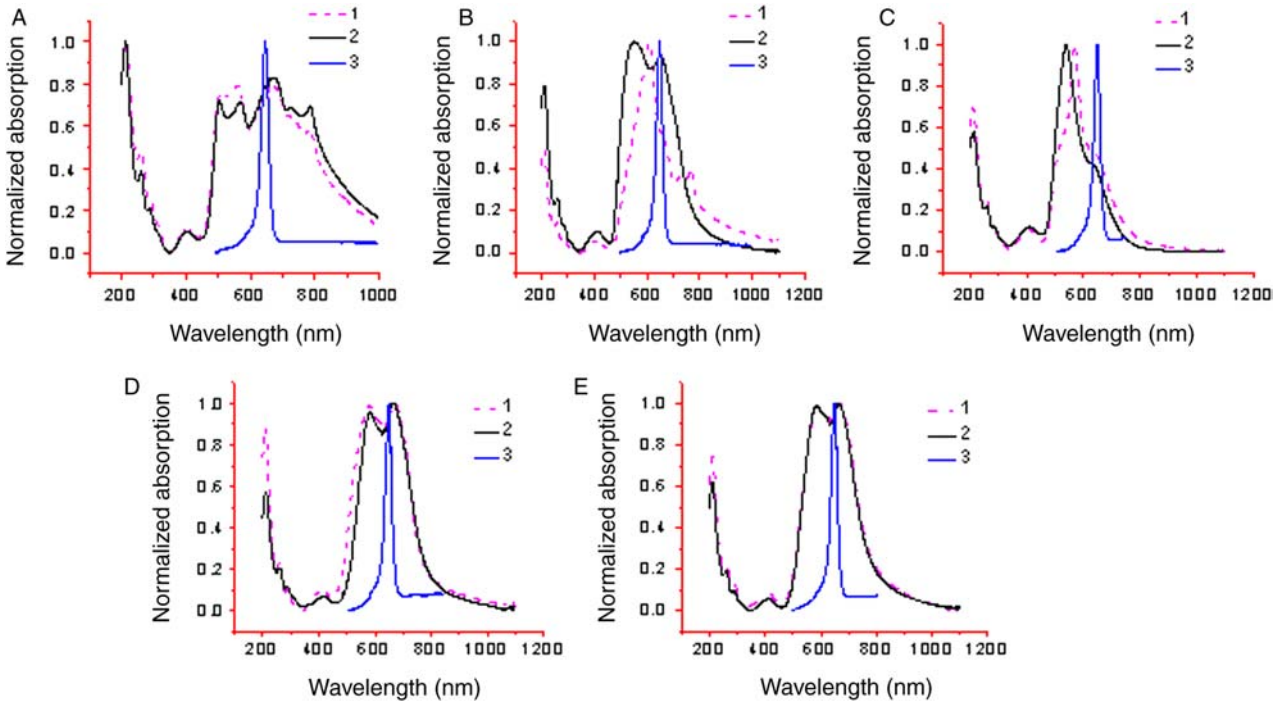


Figure 10. (A) Comparison of absorption spectra for **SQC3OH**: (1) after spin coating and thermal annealing, (2) after spin coating and (3) in $CHCl_3$ solution, $\lambda_{max} = 647$ nm. (B) Comparison of absorption spectra for **SQC4OH**: (1) after spin coating and thermal annealing, (2) after spin coating and (3) in $CHCl_3$ solution, $\lambda_{max} = 648$ nm. (C) Comparison of absorption spectra for **SQC5OH**: (1) after thermal annealing, (2) after spin coating and (3) in $CHCl_3$ solution, $\lambda_{max} = 648$ nm. (D) Comparison of absorption spectra for **SQC6OH**: (1) after thermal annealing, (2) after spin coating and (3) in $CHCl_3$ solution, $\lambda_{max} = 650$ nm. (E) Comparison of absorption spectra for **SQC7OH**: (1) after thermal annealing, (2) after spin coating and (3) in $CHCl_3$ solution, $\lambda_{max} = 653$ nm.

Rather, we observed high fluorescence quantum yields for **SQC2OH** and **SQC3OH** consistent with the literature data and with an increase in molecular rigidity for the short alkyl chain derivatives (*51*). However, the rest of the series exhibited a moderate and nearly constant fluorescence quantum yield with no significant effect as a function of alkyl chain length (Table 2). The reasonably high luminescence quantum yields suggest the potential of these dyes for bio-imaging and laser applications.

Steady-state fluorescence excitation anisotropy is another important property measured for all members of the series. This technique often reveals important information regarding electronic transitions and a molecule's rotational dynamics. A maximum excitation anisotropy value of 0.4 indicates perfectly collinear transition dipoles, i.e. the orientation of the absorption and emission transition dipole moment are parallel, which is in accordance with a strong single low-energy absorption band ($S_0 \rightarrow S_1$ transition) (*52*). Fluorescence anisotropy spectra for the series followed a consistent trend as seen in Figure 11. They are characterised by a maximum excitation anisotropy value between 0.3 and 0.4 corresponding to $S_0 \rightarrow S_1$ transitions. Upon moving to shorter wavelengths, one encounters a change in the slope of the excitation anisotropy. At *ca*. 500 nm, a negligible absorption is observed corresponding to a one-photon forbidden $S_0 \rightarrow S_2$ transition. At around 400 nm, a

Table 2. The linear and nonlinear photophysical properties for the series of squaraine dyes.

| | Molar absorptivity, $\varepsilon$ ($L\,Mol^{-1}\,Cm^{-1} \times 10^4$) | $\lambda_{max}$ $CH_3CN$ (nm) | Emission (nm) | Stokes shift (nm) | Fluorescence quantum yield |
|---|---|---|---|---|---|
| **SQC2OH** | 17 | 640 | 654 | 14 | 0.73 |
| **SQC3OH** | 24 | 643 | 658 | 15 | 0.59 |
| **SQC4OH** | 20 | 645 | 660 | 15 | 0.42 |
| **SQC5OH** | 19 | 645 | 661 | 16 | 0.40 |
| **SQC6OH** | 24 | 645 | 662 | 17 | 0.38 |
| **SQC7OH** | 19 | 653 | 665 | 12 | 0.37 |

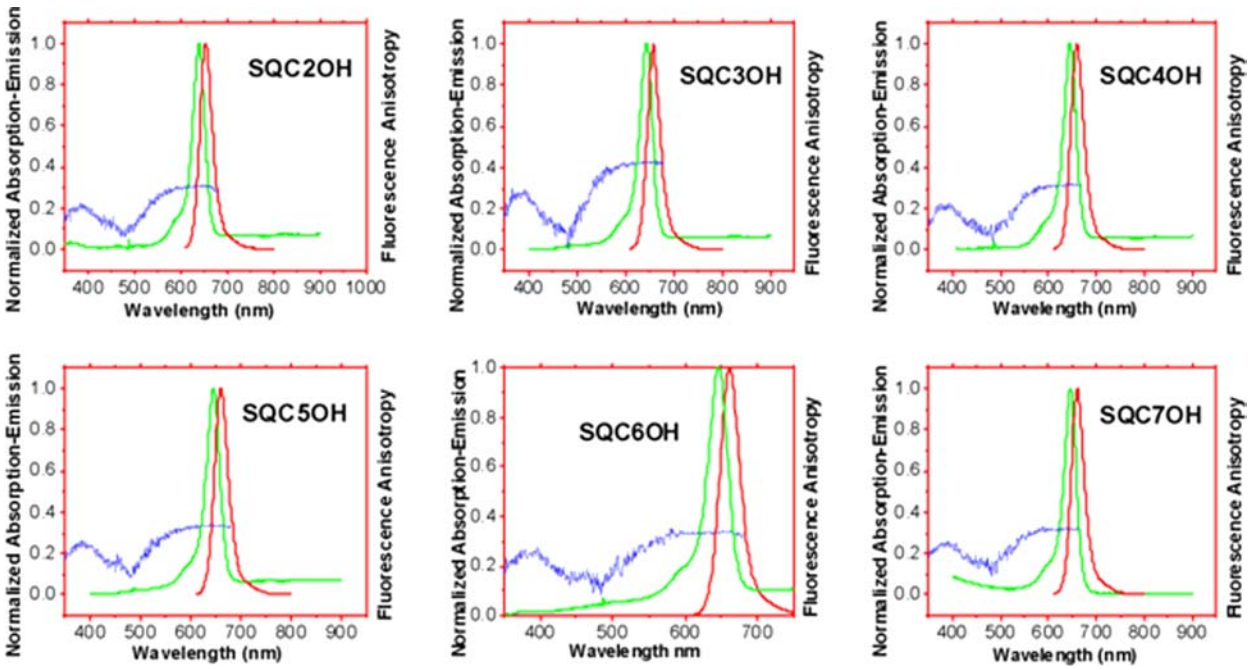


Figure 11. Normalised absorption (green), emission (red) and steady-state fluorescence excitation anisotropy (blue) spectra for the entire squaraine series. These are characterised by the maximum excitation anisotropy value approximately between 0.3 and 0.4 at long wavelength corresponding to $S_0 \rightarrow S_1$ transitions.

transition is observed corresponding to higher energy $S_0 \rightarrow S_n$ transitions.

## Conclusions

The alkyl chain in the series of squaraine compounds exerts a profound effect on the properties of these dyes. For each carbon atom added to chain, a new behaviour is revealed that is manifested in different crystalline structures and thermotropic phase transitions. The difference in crystalline structures is evident during the aggregation in the microcrystalline state: only **SQC3OH**, **SQC4OH** and **SQC5OH** formed H- and/or J-aggregates upon spin coating before and after thermal annealing owing to the formation of the herringbone structure that may account for the capability of the molecules to change the slip angle and to shift the aggregation after the annealing process. Otherwise, **SQC6OH** and **SQC7OH** exhibited only H-aggregation before and after annealing, possibly explained by having only parallel molecular arrangement in the crystal that accounts for their inability to change the slip angle and to shift their aggregation after thermal annealing treatment.

Derivatives with four (**SQC4OH**) and seven (**SQC7OH**) carbon alkyl chains triggered the formation of two LC mesophases (nematic and smectic) as determined by DSC, PLM and X-ray studies. The LC assembly was most likely influenced by the unique C—O dipole–dipole interactions between these squaraine molecules, resulting in a promising new class of liquid crystals based on the squaraine molecular structure.

Supporting Information Available. Syntheses of **SQC2OH**, **SQC3OH**, **SQC4OH**, TGA thermograms, bond length data, molecular structures derived from single-crystal X-ray crystallographic data, crystallographic data and hydrogen-bonding interaction data from X-ray crystal structures are presented.

## Acknowledgements

We wish to acknowledge the National Science Foundation (CHE-0832622 – KDB and TVT, DMR-0934212 – TVT and DMR-0520020 – PAH) and the National Academy of Sciences (PGA-P210877) for support of this work.

## References

(1) Beverina, L.; Salice, P. *Eur. J. Org. Chem.* **2010**, *7*, 1207–1225.
(2) McEwen, J.J.; Wallace, K.J. *Chem. Commun.* **2009**, *42*, 6339–6351.
(3) Umezawa, K.; Citterio, D.; Suzuki, K. *Anal. Sci.* **2008**, *24*, 213–217.
(4) Sreejith, S.; Carol, P.; Chithra, P.; Ajayaghosh, A. *J. Mater. Chem.* **2008**, *18*, 264–274.
(5) Ros-Lis, J.V.; Garcia, B.; Jimenez, D.; Martinez-Máñez, R.; Sancenon, F.; Soto, J.; Gonzalvo, F.; Valldecabres, M.C. *J. Am. Chem. Soc.* **2004**, *126*, 4064–4065.
(6) Ramaiah, D.; Eckert, I.; Arun, K.T.; Weidenfeller, L.; Epe, B. *Photochem. Photobiol.* **2004**, *79*, 99–104.

(7) Kruhlak, R.J.; Kuzyk, M.G. *J. Opt. Soc. Am. B* **1999**, *16*, 1756–1767.
(8) Terpetschnig, E.; Szmacinski, H.; Ozinskas, A.; Lakowicz, J.R. *Anal. Biochem.* **1994**, *217*, 197–204.
(9) Li, J.-R.; Li, B.-F.; Li, X.-C.; Tang, J.A.; Jiang, L. *Thin Solid Films* **1996**, *287*, 247–251.
(10) Law, K.Y. *J. Imaging Sci. Technol.* **1990**, *34*, 38–44.
(11) Toro, C.; De Boni, L.; Yao, S.; Ritchie, J.P.; Masunov, A.E.; Belfield, K.D.; Hernandez, F.E. *J. Chem. Phys.* **2009**, *130*, 2145041–2145046.
(12) Law, K.Y.; Bailey, F.C. *J. Org. Chem.* **1992**, *57*, 3278–3286.
(13) Law, K.Y.; Bailey, F.C. *Dyes Pigments* **1988**, *9*, 85–107.
(14) Law, K.Y.; Bailey, F.C. *Can. J. Chem.* **1986**, *64*, 2267–2273.
(15) Saito, K. *J. Phys. Chem. B* **2001**, *105*, 4235–4238.
(16) Dimitriev, O.P. *J. Mol. Liq.* **2005**, *120*, 131–133.
(17) Tian, M.; Furuki, M.; Iwasa, I.; Sato, Y.; Pu, L.S.; Tatsuura, S. *J. Phys. Chem. B* **2002**, *106*, 4370–4376.
(18) McKerrow, A.J.; Buncel, E.; Kazmaier, P.M. *Can. J. Chem.* **1995**, *73*, 1605–1615.
(19) Kazmaier, P.M.; Hamer, G.K.; Burt, R.A. *Can. J. Chem.* **1990**, *68*, 530–536.
(20) Crossley, M.L.; Dreisbach, P.F.; Hofmann, C.M.; Parker, R.P. *J. Am. Chem. Soc.* **1952**, *74*, 573–578.
(21) Sprenger, H.E.; Ziegenbein, W. *Angewandte Chemie* **1966**, *78*, 937–938.
(22) Schmidt, A.H.. In *Oxocarbons*; West, R., Ed.; Academic Press: New York, 1980; pp 185–231.
(23) Lynch, D.E.; Byriel, K.A. *Cryst. Eng.* **1999**, *2*, 225–239.
(24) Ashwell, G.J.; Bahra, G.S.; Brown, C.R.; Hamilton, D.G.; Kennard, C.H.L.; Lynch, D.E. *J. Mater. Chem.* **1996**, *6*, 23–26.
(25) Stawasz, M.E.; Sampson, D.L.; Parkinson, B.A. *Langmuir* **2000**, *16*, 2326–2342.
(26) Vollhardt, K.P.C.; Schore, N.E. *Organic Chemistry: Structure and Function*, 4th Ed.; W.H. Freeman & Company: New York, 1996; p 77.
(27) Gautam, S.; Choudhury, R.R.; Panicker, L.; Mitra, S.; Mukhopadhyay, R. *Chem. Phys. Lett.* **2008**, *453*, 207–211.
(28) Chakrabarti, D.; Bagchi, B. *Adv. Chem. Phys.* **2009**, *141*, 249–319.
(29) Mori, A.; Takeshita, H.; Kida, K.; Uchida, M. *J. Am. Chem. Soc.* **1990**, *112*, 8635–8636.
(30) Qaddoura, M.A.; Belfield, K.D. *Int. J. Mol. Sci.* **2009**, *10*, 4772–4788.
(31) Demus, D., Goodby, J., Gray, G.W., Spiess, H.-W., Vill, V. In *Handbook of Liquid Crystals Low Molecular Weight Liquid Crystal*, Wiley-VCH: Weinheim, 1998; pp 3–20.
(32) Mortensen, K. In *Texture of Liquid Crystal*, Wiley-VCH: Weinheim, 2004; Vol. 16.
(33) Geurst, J.A. *Phys. Lett. A* **1971**, *34*, 283–284.
(34) Chandrasekhar, S.; Ranganath, G.S. *Adv. Phys.* **1986**, *35*, 507–596.
(35) Law, K.Y.; Bailey, F.C. *Dyes Pigments* **1993**, *21*, 1–12.
(36) Law, K.Y. J. Imaging Sci. *Technol.* **1992**, *36*, 567–573.
(37) Wei, G.; Lunt, R.R.; Sun, K.; Wang, S.; Thompson, M.E.; Forrest, S.R. *Nano Lett.* **2010**, *10*, 3555–3559.
(38) Liang, K.; Law, K.-Y.; Whitten, D.G. *J. Phys. Chem.* **1994**, *98*, 13379–13384.
(39) Chudinova, G.K.; Barachevskii, V.A. *Zh. Fiz. Khim.* **1995**, *69*, 1311–1314.
(40) Tanaka, M.; Sekiguchi, T.; Matsumoto, M.; Nakamura, T.; Manda, E.; Kawabata, Y. *Thin Solid Films* **1988**, *160*, 299–302.
(41) Kim, S.; Furuki, M.; Pu, L.S.; Nakahara, H.; Fukuda, K. *J. Chem. Soc., Chem. Commun.* **1987**, (16), 1201–1203.
(42) Ashwell, G.J.; Williamson, P.C.; Green, A.; Bahra, G.S.; Brown, C.R.; Aust *J. Chem.* **1998**, *51*, 599–604.
(43) Ashwell, G.J.; Jefferies, G.; Rees, N.D.; Williamson, P.C.; Bahra, G.S.; Brown, C.R. *Langmuir* **1998**, *14*, 2850–2856.
(44) Ashwell, G.J. *J. Mater. Chem.* **1998**, *8*, 373–376.
(45) Tani, T. In *J-Aggregates*; Kabayashi, T., Ed.; World Scientific Publishing: Singapore, 1996; pp 209–228.
(46) Scherer, P.O.J. In *J-Aggregates*; Kabayashi, T., Ed.; World Scientific Publishing: Singapore, 1996; pp 95–110.
(47) Knoester, J.; Spano, F.C. In *J-Aggregates*; Kabayashi, T., Ed.; World Scientific Publishing: Singapore, 1996; pp 111–160.
(48) Servaites, J.D.; Yeganeh, S.; Marks, T.J.; Ratner, M.A. *Adv. Funct. Mater.* **2010**, *20*, 97–104.
(49) Afolabi, O.M.; Ajayi, I.R.; Siyanbola, W.O. *Global. J. Pure Appl. Sci.* **2004**, *10*, 435–439.
(50) Wojtyk, J.; McKerrow, A.; Kazmaier, P.; Buncel, E. *Can. J. Chem.* **1999**, *77*, 903–912.
(51) Law, K.Y.J. *Phys. Chem.* **1987**, *91*, 5184–5193.
(52) Lepkowicz, R.S.; Cirloganu, C.M.; Przhonska, O.V.; Hagan, D.J.; Van Stryland, E.W.; Bondar, M.V.; Slominsky, Y.L.; Kachkovski, A.D.; Mayboroda, E.I. *Chem. Phys.* **2004**, *306*, 171–183s.